Three-dimensional dispersion induced by extreme tensile strain in $La_{2-x}Sr_xCuO_4$ films

D. Cloetta,[1] D. Ariosa,[1] C. Cancellieri,[1] M. Abrecht,[2] S. Mitrovic,[3] and D. Pavuna[1]
[1]*Institute of Physics of Complex Matter, EPFL, CH-1015 Lausanne, Switzerland*
[2]*University of Wisconsin, 3731 Schneider Drive, Stoughton, Wisconsin 53789, USA*
[3]*Department of Physics, California Institute of Technology, Pasadena, California 91125, USA*
(Received 23 May 2006; revised manuscript received 27 June 2006; published 31 July 2006)

The electronic band structure probed by angle-resolved photoemission spectroscopy on thin epitaxial $La_{2-x}Sr_xCuO_4$ films under extreme tensile strain shows anomalous features compatible with *c*-axis dispersion. This result is in striking contrast with the usual quasi-two-dimensional (2D) dispersion observed up to now in most superconducting cuprates, including relaxed and compressively strained $La_{2-x}Sr_xCuO_4$ films grown under the same conditions. The data were analyzed using a 3D tight-binding dispersion for a body-centered-tetragonal lattice. We relate the enhancement of the *c*-axis dispersion to the significant displacement of the apical oxygen induced by epitaxial strain.

DOI: 10.1103/PhysRevB.74.014519 PACS number(s): 74.78.Bz, 68.60.Bs, 79.60.−i

I. INTRODUCTION

High-temperature superconductors (HTSCs) are very sensitive to variations of the lattice parameters. The study of correlations between lattice distortions, electronic structure, and superconducting properties is of central interest in the search for the still unknown pairing mechanism. In particular, the variations of the superconducting critical temperature T_C for bulk samples under hydrostatic pressure,[1] as well as for epitaxially strained thin films,[2,3] have been widely studied during the last 15 years. More recently, compared to the bulk crystal,[4] angle-resolved photoemission spectroscopy (ARPES) studies on $La_{2-x}Sr_xCuO_4$ (LSCO) thin films under in-plane compressive epitaxial strain[5] show significant and unexpected changes in the band dispersion: the two-dimensional (2D) Fermi surface changes from "holelike" to "electronlike" reducing the density of states (DOS) near the Fermi energy (E_F) with a concomitant enhancement of T_C. In this paper, we present ARPES measurements on LSCO thin films grown with the opposite in-plane strain (tensile). The T_C for moderately tensile-strained films is strongly reduced and can even be suppressed for higher strain. ARPES data taken for one photon energy cannot be explained by the conventional 2D dispersion observed for unstrained and compressively strained LSCO films. However, differences in the dispersions and the Fermi surfaces from predictions of a 2D tight-binding model can be accounted for under the assumption of a 3D dispersion in the model. Furthermore, analyzed within a 3D tight-binding (3D TB) approach, the data show important hopping contributions up to the next nearest neighbor out of plane, denoting a dramatic rearrangement of atomic orbitals within the LSCO unit cell. We propose that these observed effects are related to the significant displacement of the apical oxygen, induced by the epitaxial strain.

In Sec. II we describe the growth and the structural characterization of in-plane tensile-strained LSCO films. In Sec. III we present the results obtained on these films by ARPES. Section IV is devoted to the analysis and discussion of the data. Finally, we summarize our findings and draw conclusions in Sec. V.

II. GROWTH AND CHARACTERIZATION

LSCO thin films were grown on (100) $SrTiO_3$ (STO) substrates by pulsed laser ablation technique using a neodymium-doped yttrium aluminum garnet (Nd-YAG) laser with a repetition rate of 3.3 Hz and a wavelength of 266 nm. The energy per pulse was 100 mJ. The oxygen pressure during the deposition of the film was 300 mTorr; afterward it was increased to 1 atm for the annealing treatment. The deposition conditions were chosen in order to provide the best quality of the films to perform ARPES measurements. In particular, the surface quality is extremely crucial for photoemission analysis. In order to reduce the roughness and the number of defects, we deposited all the films using off-axis geometry.[6,7] The substrates were chosen according to the level and the type of strain one wants to impose on the films. We used STO or $SrLaGaO_4$ (SLGO) to induce tensile strain and $SrLaAlO_4$ for the compressive strain. All the deposited films were characterized structurally and electrically. We used x-ray diffraction to determine the level of strain, the orientation of our films, their thickness, and their in-plane coherence length. From peak positions in θ-2θ scans, we determined the *c*-axis compression and thus the in-plane tensile strain. The emergence of finite-size oscillations as shown in Fig. 1(a) is not only an indication for good surface quality; they can also be used to estimate the film thickness by fitting them and adjusting the number of unit cells until it matches the measurement. The *c*-axis compression can be changed by varying the film thickness. Our thinnest film, corresponding to 3.5 unit cells, had a *c* axis of 13.06 Å, i.e., a *c*-axis strain $\epsilon_c = -1.2\%$ (compression). Using available data for the elastic moduli of LSCO,[8] one can estimate the corresponding in-plane strain $\epsilon_{ab} = +3.3\%$ (for Poisson ratio $\nu \approx 0.2$). This unusual huge in-plane expansion of the lattice coincides with the relative mismatch between the STO substrate and the LSCO film. This should result in a perfect lattice matching without misfit dislocations. Indeed, for thin films below 5 unit cells under tensile strain, the rocking curves [see Fig. 1(b)] have a full width at half maximum (FWHM) of about 0.03 to 0.05, corresponding to the instrumental resolution. This corroborates not only the high quality of the film, but

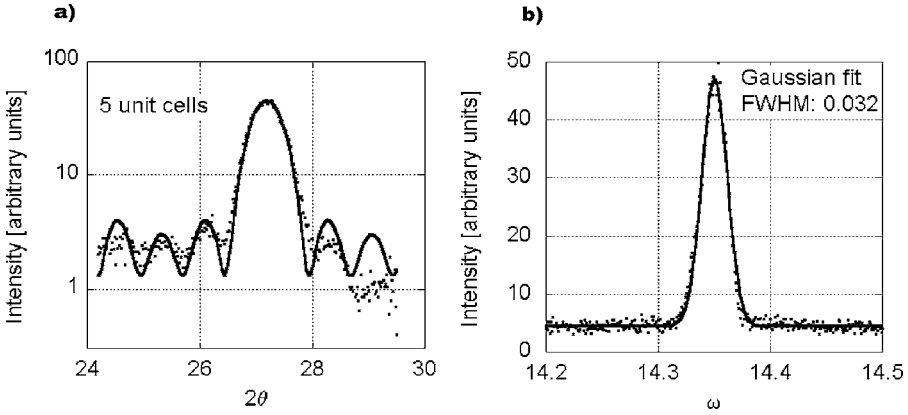

FIG. 1. (a) Finite-size oscillations used to estimate the film thickness; (b) rocking curve around (004).

also the accuracy of our estimation for the in-plane strain ϵ_{ab}. Resistivity as well as magnetic susceptibility measurements were also systematically performed on our films. T_C was strongly reduced under strain and even completely suppressed for extreme tensile strain.

III. ARPES

Our ARPES measurements were performed at the Synchrotron Radiation Center in Wisconsin on the 6 m PGM beamline. The photon energy can be chosen in a range between 8 and 245 eV. The sample is situated in an ultrahigh vacuum ($<10^{-10}$ Torr) chamber and is mounted on a cold finger, which can be cooled down to 11 K. For the ARPES measurements on $La_{2-x}Sr_xCuO_4$ films under tensile strain we used a SCIENTA SES 2002, with an energy resolution of 15 meV and a momentum resolution of 0.04 $Å^{-1}$. The analyzer was oriented for horizontal polarization. Due to the weakness of the signal, it was much more difficult to obtain ARPES spectra and moreover to analyze the data for films under tensile strain than for films under compressive strain, presumably due to the bigger lattice mismatch and the subsequent increased amount of dislocations in the case of films under moderate tensile strain.

The ten films under tensile strain exhibiting a dispersing signal have a c axis of about 13.1 Å, corresponding to a compression of 1% and to strong in-plane tensile strain, as discussed previously. The most successful measurements have been performed on LSCO films grown on STO, but a dispersion could also be observed on films grown on SLGO substrates. The overdoped film (x=0.20), presented and discussed here, has been grown on STO. Measurements have been performed at the photon energy of 60 eV for the angles φ=0 (Γ-X), 5, 10, 30, and 45 (Γ-M) as depicted in Fig. 2. The sample was cooled at 11 K during data acquisition. In Fig. 3, the ARPES measurements are shown in the momentum distribution curve (MDC) representation.

IV. ANALYSIS

Usually, when dealing with superconducting cuprates, ARPES data are analyzed on the basis of 2D band models. In particular, the Fermi surface (FS) is assumed to be "cylindrical" [see Fig. 4(a)]. Its projection in the 2D reciprocal space is the k_z-independent Fermi contour (FC) given by the points where the band intersects E_F. According to Luttinger's rule,[9] the FC should enclose a fraction of the total 2D Brillouin zone (BZ) equal to the band filling ratio. In terms of the hole doping x (holes per Cu atom), the enclosed surface S_{in} should obey

$$x = 1 - 2\frac{S_{in}}{S_{BZ}}, \tag{1}$$

where S_{BZ} stands for the total area of the BZ. When applying this scheme to our data on in-plane tensile-strained LSCO films, we obtain a hole doping of about −0.2, i.e., high electron doping. This result is in absolute contradiction with the nominal hole doping value of our sample (x=0.20) determined essentially by its Sr content. The departure from the nominal value is too large to be considered as a small perturbation due to oxygen and/or strontium stoichiometry. In fact, in order to obtain electron doping in the LSCO (La-214) structure, one would have to introduce substantial chemical modifications, for example[10] replacing La(+3) with Ce(+4) instead of Sr(+2). In any case, even accepting these doping values, the band dispersion $E(\vec{k})$ cannot be fitted within 2D models. Indeed, the usual phenomenological 2D tight-binding dispersion,[11] successfully used for both relaxed and in-plane compressively strained films,[5] failed in the tensile case: the parameters defining the 2D dispersion varied sig-

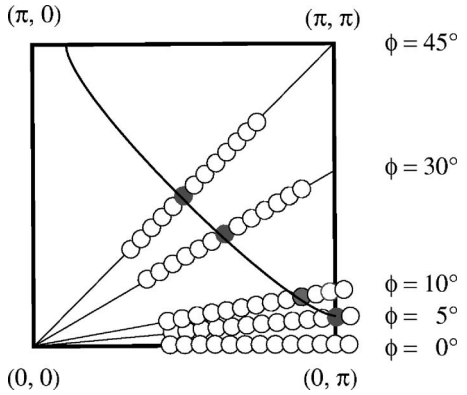

FIG. 2. Typical measured paths in the right upper quadrant of the BZ. Gray circles indicate the points where the dispersion crosses the Fermi energy.

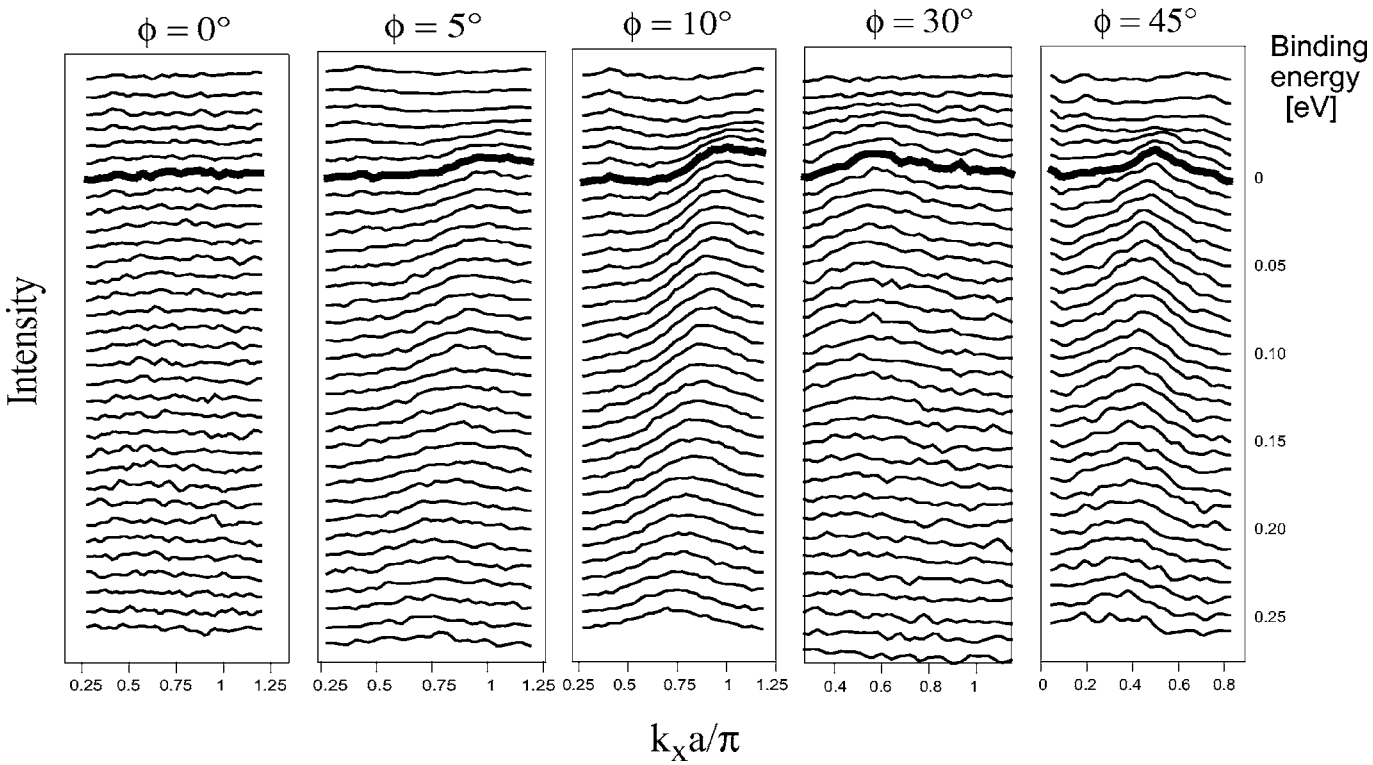

FIG. 3. MDCs for different angles, from an overdoped film under extreme tensile strain. The data were taken at a photon energy E_{PH}=60 eV.

nificantly from one direction (φ) of the 2D BZ to another. As we shall see in the following, the above contradictions can only be removed by considering a 3D band dispersion for our tensile strained films.

Since we were expecting the usual 2D band dispersion, ARPES measurements were performed at constant photon energy (CPE), namely, E_{PH}=60 eV. Thus, our data are definitively not sufficient to experimentally map the 3D dispersion. However, using the collected data, we have chosen to perform a rough reconstruction of the band structure based on a 3D TB approach. This "zero-order approximation" of the band structure can be used for the design of further

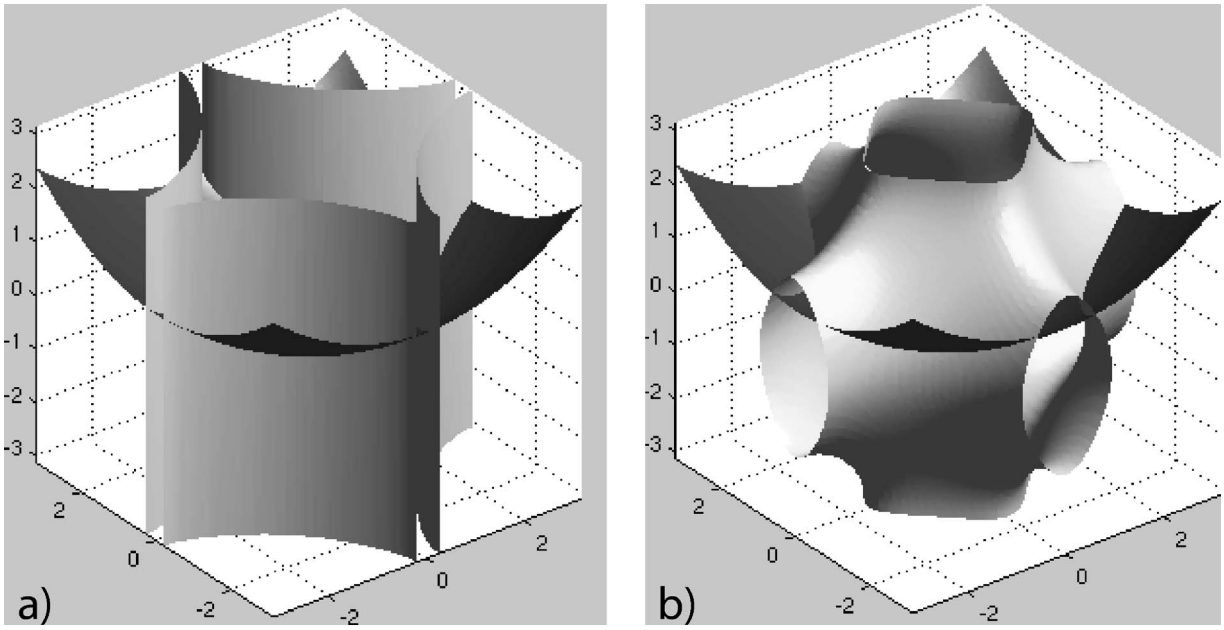

FIG. 4. Example for intersections of the Fermi surface (light) with the Fermi probing sphere (dark) for 2D (a) and 3D (b) band dispersion, in the case of a simple tetragonal lattice.

ARPES experiments on tensile-strained films. In order to realize the above program, we have to deal with two major difficulties: (a) the nonconservation of the photoelectron wave vector at the sample surface and (b) the definition of a suitable model for the 3D dispersion.

For the determination of the normal component k_z of the wave vector in the initial state, we have used the nearly-free-electron approximation for the electron in the excited state, with an adjustable effective mass. Concerning the model, we have extended the 2D TB approach to 3D. The proposed dispersion is as general as possible, in the sense that it can be considered as a particular truncation of the Fourier expansion for a general 3D periodic dispersion, regardless of any *a priori* consideration about particular microscopic models.

A. CPE measurements

The following approach for mapping the 3D dispersion follows essentially the textbook by Hüfner on photoemission spectroscopy.[12] The magnitude of the initial in-plane wave vector (conserved through the sample surface) can be computed, as usual, from the measurements

$$k_{\parallel} = \sqrt{\frac{2mE_K}{\hbar^2}}\sin(\theta) = 0.512\sqrt{E_K}\sin(\theta). \tag{2}$$

For the photoelectron in the final state (still within the solid), the initial in-plane wave vector is conserved modulo a reciprocal lattice vector $\vec{G}$. For extraction angles small enough ($\theta < 15°$), this vector is perpendicular to the surface. Indeed, for those angles the in-plane conserved wave vector belongs to the first 2D BZ. Thus the normal component $K_{\perp} = k_{\perp} + G_{\perp}$ (reduced when traveling through the surface) can be written (in the nearly-free-electron approximation) as follows:

$$K_{\perp} = \sqrt{\frac{2m^*}{\hbar^2}}\sqrt{E_K\left(1 - \frac{m}{m^*}\sin^2(\theta)\right) + \phi + |E_0|} \tag{3}$$

where $|E_0|$ is the energy at the bottom of the free-electron parabola with respect to the Fermi level, ϕ is the work function, and m^* is the effective mass of the excited electron within the solid. For the fit, we have chosen an inner potential[13] (including the work function) $V_0 = \phi + |E_0|$ in the interval 10–14 eV, in agreement with the values found in the literature for similar oxides.[14,16] Both V_0 and m^* were adjusted during the fitting procedure, converging to 13 eV and $1.38m_e$, respectively.

The reciprocal lattice vector $\vec{G} = G_{\perp}\hat{z}$ is estimated, for each photon energy, by considering the normal emission: $G_{\perp} \approx \sqrt{\frac{2m^*(E_{PH}+|E_0|)}{\hbar^2}}$. If the calculated vector lies in the $(n+1)$th BZ along the normal direction, one can write $G_{\perp} = n\frac{4\pi}{c}$ for any detected electron leaving the surface with the in-plane momentum lying in the first 2D BZ (the 4π comes from the doubling of the z-axis period of the fct BZ as discussed in the next section). In our case $E_{PH} = 60$ eV, $|E_0| = 8.6$ eV, and $m^* = 1.38m_e$; thus $n = 5$.

From the above description, one can see that ARPES measurements, using constant photon energy, probes the 3D reciprocal space on a particular surface defined by

$$k_{\parallel}^2 + (k_{\perp} + G_{\perp})^2 = \frac{2m^*}{\hbar^2}(E_{PH} + |E_0| + E_b). \tag{4}$$

For each given binding energy E_b, Eq. (4) is the equation of a sphere centered at $(0,0,-G_{\perp})$. In the following, we will call it the "CPE-probing sphere." The probing sphere is located between two concentric spheres with slightly different radius: $\sqrt{\frac{2m^*[E_{PH}+|E_0|+E_b(0)]}{\hbar^2}}$ for the maximal binding energy (Γ point), and $\sqrt{\frac{2m^*(E_{PH}+|E_0|)}{\hbar^2}}$ for zero binding energy (Fermi level). Each dispersion peak in the spectrum corresponds then to an initial state wave vector $\vec{k}$ lying on the intersection of the probing sphere (4)—for the measured binding energy E—with the constant energy surface $E_b(\vec{k}) = E$.

This intersection, for zero binding energy, when projected on the (k_x, k_y) plane, is precisely the observed Fermi contour. When working with 2D materials, there is no $k_{\perp}$ dependence in the binding energies. Constant energy surfaces are then vertical cylinders, and their intersection with any probing sphere gives always the same planar projection [Fig. 4(a)]. For 3D dispersive materials, the situation is quite different [Fig. 4(b)]: the Fermi contours can display very tortuous shapes, varying from one photon energy to another, depending on the local shape of the Fermi surface at its intersection with the Fermi probing sphere (4). It is then clear that the naive 2D version of Luttinger's rule no longer applies in this context.

B. Fitting with 3D TB dispersion for a bct lattice

As for 2D bands, the TB approach for a 3D lattice can be viewed as the special truncation of a Fourier series for the conduction band dispersion $E(\vec{k})$, a periodic function in the reciprocal space. LSCO has a body-centered-tetragonal (bct) structure. The primitive cell of such a lattice is defined trough the following translation vectors:

$$\vec{a}_1 = (a,0,0), \quad \vec{a}_2 = (0,a,0), \quad \vec{a}_3 = \left(-\frac{a}{2}, -\frac{a}{2}, \frac{c}{2}\right). \tag{5}$$

The corresponding primitive vectors in the face-centered-tetragonal (fct) reciprocal lattice are then

$$\vec{b}_1 = \left(\frac{2\pi}{a}, 0, \frac{2\pi}{c}\right), \quad \vec{b}_2 = \left(0, \frac{2\pi}{a}, \frac{2\pi}{c}\right), \quad \vec{b}_3 = \left(0, 0, \frac{4\pi}{c}\right). \tag{6}$$

Notice the doubled extension of the reciprocal lattice along the z axis, compared with the BZ of the simple tetragonal lattice depicted in Fig. 4(b). In 3D, the most general expression for $E(\vec{k})$ is

$$E(\vec{k}) = \sum_{n_1,n_2,n_3} E_{n_1,n_2,n_3} \exp[i\vec{k}\cdot(n_1\vec{a}_1 + n_2\vec{a}_2 + n_3\vec{a}_3)], \tag{7}$$

where $\vec{k}$ is the wave vector of the electron in the conduction band and (n_1,n_2,n_3) are three integers specifying a general translation vector in the direct lattice. The periodicity of ex-

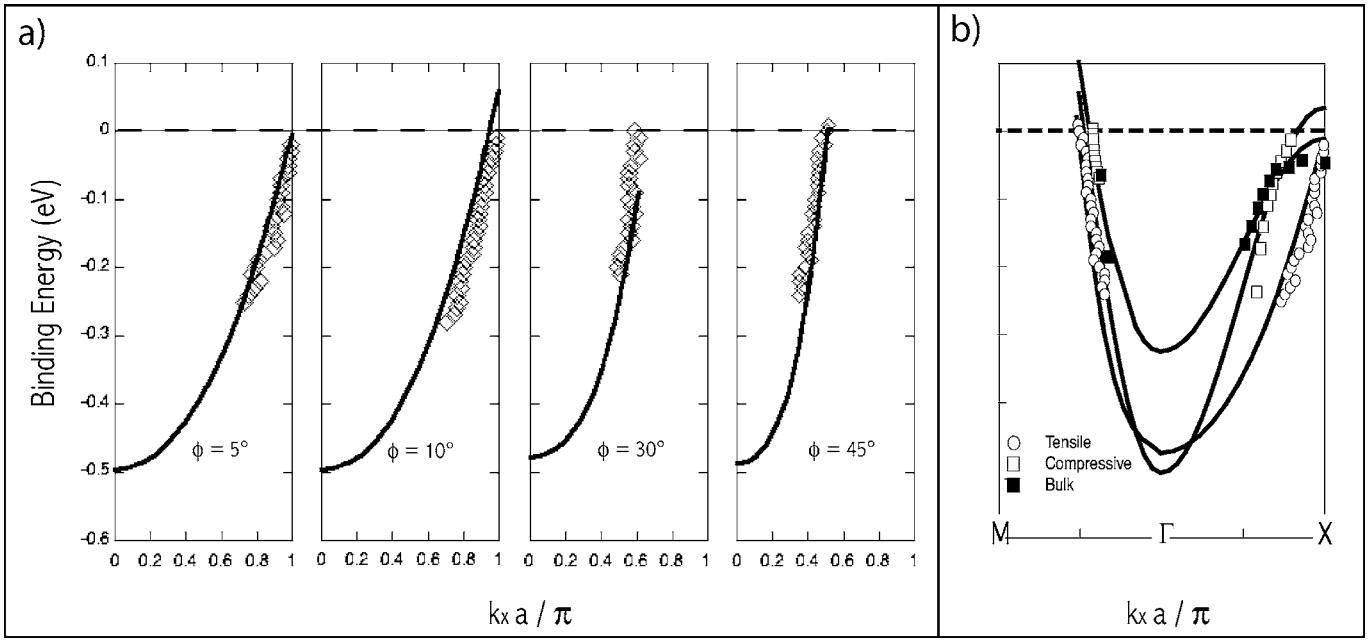

FIG. 5. (a) 3D band fit for overdoped sample (x=0.2). Fitting parameters: m^*/m_e=1.38; $|E_0|$=8.6 eV; t=0.17 eV; r=0.26; ν=0.6; ν'=0.2. (b) Band dispersions along Γ-X and Γ-M directions for bulk (black squares), compressive strained films (white squares), and tensile-strained films (white circles) and their respective TB fits.

pression (7) in the reciprocal space is easy to check: $E(\vec{k})$ remains unchanged after the addition of any primitive vector of the reciprocal space to the electron wave vector $\vec{k}$.

The simplest 3D TB approximation would consist of retaining hopping terms up to the second neighbor, both in and out of plane. Thus, we chose the indices n_i such that the sum runs over the four in-plane nearest neighbors (NNs) $(\pm a,0,0);(0,\pm a,0)$, the four in-plane next-nearest neighbors (NNNs) $(\pm a,\pm a,0)$, the eight out-of-plane NNs $(\pm\frac{a}{2},\pm\frac{a}{2},\pm\frac{c}{2})$, and the two out-of-plane NNNs $(0,0,\pm c)$.

The coefficients affecting the in-plane terms are usually denoted as t and t', for the NN and NNN hopping, respectively. We will use the notation t'' and t''' for the NN and NNN out-of-plane contributions. Since we are interested in the binding energies $E_b(\vec{k})=E(\vec{k})-E_F$, by properly choosing the energy axis we can finally write the general TB expression for the bct 3D band structure as follows:

$$E_b(\vec{k}) = (\mu - E_F) - 2t[\cos(k_x a) + \cos(k_y a)] + 4t' \cos(k_x a)\cos(k_y a) - 8t'' \cos\left(\frac{k_x a}{2}\right)\cos\left(\frac{k_y a}{2}\right)\cos\left(\frac{k_z c}{2}\right) + 2t''' \cos(k_z c). \quad (8)$$

Expression (8) contains the 2D TB expression with additional terms coming from out-of-plane contributions. Due to the periodicity along the third axis, the integral of $E_b(\vec{k})$ over k_z in the first BZ is the 2D restriction of the dispersion [also obtained from Eq. (8) by making t''=0 and t'''=0]. Thus, Luttinger's rule as stated in Eq. (1) applies for the 2D restriction (but not for the FC) and provides us with a relationship between μ, E_F, t, and t'. Given the values of the ratio $r=t'/t$ and the doping x, there is only a single value of $(\mu-E_F)/t$ compatible with Eq. (1). Expanded linearly in r about half filling, the relation reads $(\mu-E_F)/t=2x+2.24r$. Since we know the Sr content x of our films, the effective number of adjustable parameters is reduced to 4. For simplicity, as well as the ratio r, we introduced the following dimensionless parameters: $\nu=t''/t$ and $\nu'=t'''/t$.

The measured dispersions for four in-plane orientations $(\varphi=5°,10°,30°,45°)$ were fitted using Eqs. (2), (3), and (8). Figure 5(a) shows the fits obtained for an overdoped (OD) sample (x=0.20). In Fig. 5(b), we have superimposed the measured dispersions along Γ-X ($\varphi=0\pm5°$) and Γ-M ($\varphi=45°$) for three types of samples: bulk relaxed,[4] compressive,[5] and tensile-strained films. It is clear from Fig. 5(b) that the main visible differences are in the antinodal direction (Γ-X) and for the tensile-strained case. While the bulk and compressive-strained sample data are easily fitted with the 2D TB dispersion, the unusual curvature of the band for the tensile case cannot be reproduced by any 2D TB fit. Starting with values close to the 2D band parameters found in previous measurements for OD relaxed LSCO films,[5] we achieved the best fit by essentially switching on the out of plane coefficients. The value of the in-plane NN hopping term t is just 25% larger than the value found for the bulk, while the ratio r remains unchanged. Beside the 3D character of the dispersion, which makes LSCO films under in-plane tensile strain different from bulk and compressively strained films, the most striking quantitative feature of the fits in Fig. 5 is the significant value of the out-of-plane contributions. The fit is reliable in the sense that the adjustment of the fitting parameters is very sensitive, since we have to fit simultaneously—with a single set of band parameters—four different dispersion curves corresponding to four different

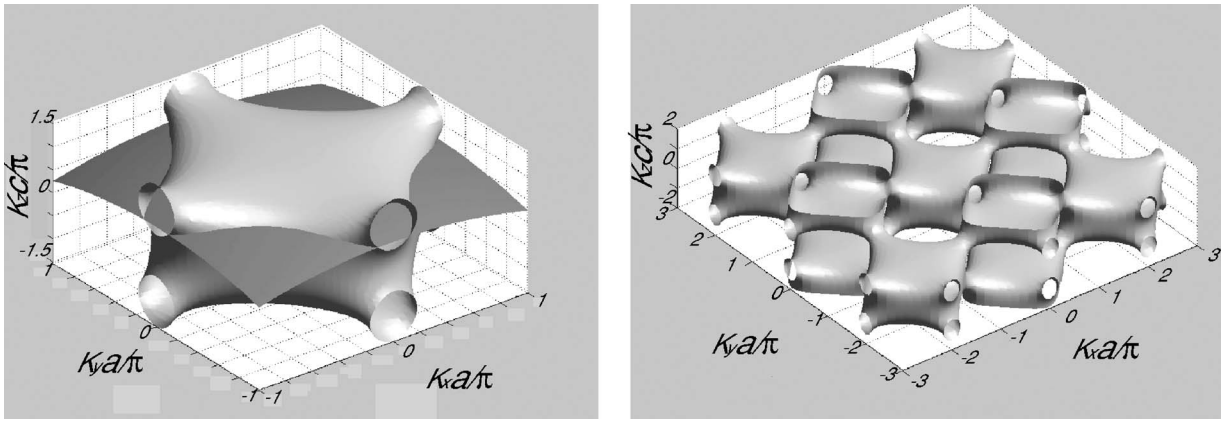

FIG. 6. Reconstructed Fermi surface according to the fits in Fig. 5, and its intersection with the Fermi probing sphere (left). Representation of the FS in the repeated-zone scheme (right).

measuring paths in the reciprocal space (Fig. 2). Thus, in the framework of the 3D TB approach, we conclude that in-plane tensile strain: (i) affects marginally the overlap between Cu $3d_{x^2-y^2}$ and O $2p_x$ as well as between O $2p_x$ and O $2p_y$ orbitals, responsible for in-plane hopping, and (ii) triggers out-of-plane dispersion, presumably due to a significant rearrangement of out-of-plane atomic orbitals. This effect is not at all surprising, considering the huge *c*-axis contraction of the unit cell.

Concerning the 3D dispersion, as already shown by Pavarini *et al.*,[11] the k_z dispersion in the La-214 family comes from the apical oxygen p_z and Cu $3d_{z^2-1}$ character, and it is enhanced as the Cu to apical oxygen distance is reduced. In all other HTSCs, these two bands hybridize far less with the conduction band than does the Cu *s* band. Thus, in our films, extreme in-plane tensile strain (*c*-axis contraction), by reducing the Cu to apical oxygen distance, is responsible for the observed enhancement of the k_z dispersion.

It is interesting to relate our findings on La-214 to recent theoretical work on 3D dispersion in HTSCs,[15] and observed 3D dispersion in overdoped $Bi_2Sr_2CuO_{6+\delta}$ (Ref. 16) and $Tl_2Ba_2CuO_{6+\delta}$ crystals.[17]

In the left part of Fig. 6, we have plotted the reconstructed 3D FS and its intersection with the Fermi probing sphere for E_{PH}=60 eV, for which we have used the same band parameters as in the dispersion fits. The right part of Fig. 6 is the FS drawn in the repeated-zone scheme in order to illustrate the fct symmetry of the reciprocal lattice. The calculated FC for a photon energy of 60 eV is shown in Fig. 7(a). It is located between two planar cuts of the FS (for k_z=0 and π/c) and fits well the experimental Fermi crossing points. In Fig. 7(b) we plotted together the calculated FC's based on the dispersion fits for a bulk sample (dotted line), a compressively strained film[5] (thin continuous line), and a tensile-strained film (thick continuous line). For comparison, we drew a diamondlike shadow region representing the area of occupied states for a hypothetical half-filled band sample with electron-hole symmetry, i.e., with t'=0. From Fig. 7(b), it is evident that the relaxed and compressively strained samples have similar hole doping, while the tensile-strained film seems electron doped, apparently violating Luttinger's rule as discussed previously.

V. CONCLUSIONS

Single-photon-energy ARPES measurements, made on pulsed laser deposition grown epitaxial LSCO thin films under extreme in-plane tensile strain, support a 3D dispersion scenario. These results are in clear contrast with those obtained previously for films under compressive strain. While in-plane compressive strain affected essentially in-plane hopping probabilities (the t' diagonal term was almost sup-

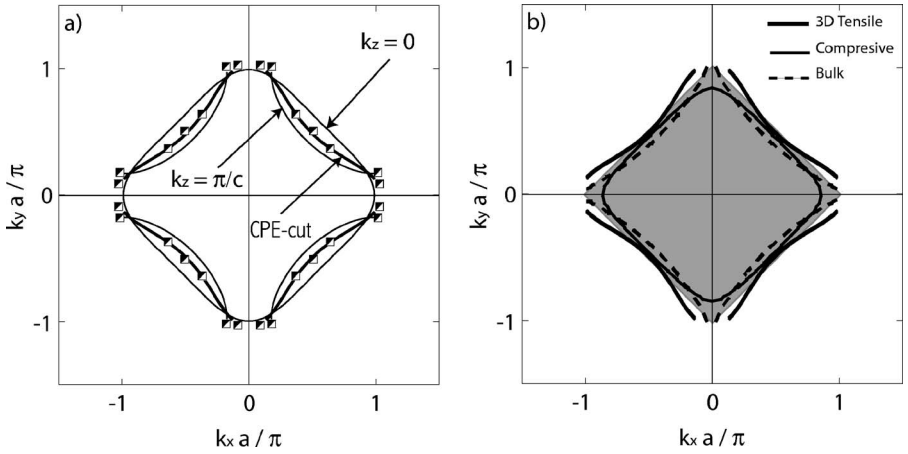

FIG. 7. (a) Calculated FC (CPE cut) and two particular planar cuts at k_z=0 and π/c. The experimental Fermi crossing points (diamonds) have been reproduced from the first octant by symmetry. (b) Calculated FCs based on dispersion fits for bulk sample (dotted line), compressively strained film (thin continuous line), and tensile-strained film (thick continuous line). The diamondlike shadow region represents the area of occupied states for a hypothetical half-filled band sample.

pressed), the tensile strain leaves the in-plane terms almost unchanged but switches on dispersion along the third axis. The T_C of these films is strongly reduced, when not suppressed. The observed huge *c*-axis contraction (1%) with the resulting displacement of the apical oxygen toward the CuO_2 layer is presumably the key for understanding this unexpected effect. Indeed, it is easy to conceive that apical oxygen p_z and Cu $3d_{z^2-1}$ hybridization will be favored under such lattice distortion. More ARPES work with different photon energies is planned in order to refine the 3D Fermi surface obtained here from the fit of the measured dispersions.

ACKNOWLEDGMENTS

This work was supported by the Swiss National Science Foundation and by the EPFL. This work is based upon research conducted at the Synchrotron Radiation Center, University of Wisconsin—Madison, which is supported by the NSF under Grant No. DMR-0537588.

[1] L. Gao, Y. Y. Xue, F. Chen, Q. Xiong, R. L. Meng, D. Ramirez, C. W. Chu, J. H. Eggert, and H. K. Mao, Phys. Rev. B **50**, 4260 (1994).
[2] G. L. Belenky, S. M. Green, A. Roytburd, C. J. Lobb, S. J. Hagen, R. L. Greene, M. G. Forrester, and J. Talvacchio, Phys. Rev. B **44**, 10117 (1991).
[3] J.-P. Locquet, J. Perret, J. Fompeyrine, E. Mächler, J. W. Seo, and G. Van Tendeloo, Nature (London) **394**, 453 (1998).
[4] A. Ino, C. Kim, M. Nakamura, T. Yoshida, T. Mizokawa, A. Fujiimori, Z.-X. Shen, T. Kakeshita, H. Eisaki, and S. Uchida, Phys. Rev. B **65**, 094504 (2002).
[5] M. Abrecht, D. Ariosa, D. Cloetta, S. Mitrovic, M. Onellion, X. X. Xi, G. Margaritondo, and D. Pavuna, Phys. Rev. Lett. **91**, 057002 (2003).
[6] D. Ariosa, M. Abrecht, D. Pavuna, and M. Onellion, Proc. SPIE **4058**, 129 (2000).
[7] M. Abrecht, T. Schmauder, D. Ariosa, O. Touzelet, S. Rast, M. Onellion, and D. Pavuna, Surf. Rev. Lett. **7**, 495 (2000).
[8] J. Dominec, Supercond. Sci. Technol. **6**, 153 (1993).
[9] J. M. Luttinger, Phys. Rev. **119**, 1153 (1960).
[10] M. Naito, S. Karimoto, and A. Tsukada, Supercond. Sci. Technol. **15**, 1663 (2002).
[11] E. Pavarini, I. Dasgupta, T. Saha-Dasgupta, O. Jepsen, and O. K. Andersen, Phys. Rev. Lett. **87**, 047003 (2001).
[12] S. Hüfner, *Photoelectron Spectroscopy: Principles and Applications* (Springer-Verlag, Berlin, 2003).
[13] A. Damascelli, Phys. Scr., T **109**, 61 (2004).
[14] M. Shi, M. C. Falub, P. R. Willmott, J. Krempasky, R. Herger, K. Hricovini, and L. Patthey, Phys. Rev. B **70**, 140407(R) (2004).
[15] A. Bansil, M. Lindroos, S. Sahrakorpi, and R. S. Markiewicz, Phys. Rev. B **71**, 012503 (2005).
[16] T. Takeuchi, T. Kondo, T. Kitao, H. Kaga, H. Yang, H. Ding, A. Kaminski, and J. C. Campuzano, Phys. Rev. Lett. **95**, 227004 (2005).
[17] N. E. Hussey, M. Abdel-Jawad, A. Carrington, A. P. Mackenzie, and L. Balicas, Nature (London) **425**, 814 (2003).